Euler-Lagrange simulation of invert concrete abrasion

Tomoo Fukuda and Shoji Fukuoka

Abstract

This paper develops a new sub-particle scale abrasion model for the Concrete Discrete Element Method (CDEM). The concrete abrasion model estimates the fracture rates of concrete particles in the CDEM method based on the mechanical energy, which the moving particles consume by collisions. The present concrete abrasion model is incorporated into the APM (Arbitrary Particle Multiphase) code (Fukuoka *et al*. 2004), which is capable of simulating three-dimensional motions of arbitrarily shaped particles and water, based on the high-resolution Euler-Lagrange strategy. The APM code with the CDEM method and the new abrasion model (APM-CDEMA) was used to simulate concrete invert abrasion in a real scale abrasion experiment conducted by Fukuoka *et al*. (2004). The simulation results for the abrasion speed of concrete invert agreed well with the results of the experiment.

Keywords: sub-particle scale abrasion model, DEM, high-resolution Euler-Lagrange simulation, concrete abrasion, energy balance.

1   Introduction

Violent flows of highly concentrated water and gravel mixtures in sediment bypass tunnels make concrete inverts abrade severely. As the abrasion progresses, sediment flows concentrate on concave abrasion points and further increase the scale of the abrasion at these points. Therefore, the abrasion and motion of flows and particles interact with each other. In several studies, the abrasion volume was connected with the energy loss of moving particles during collisions with the concrete surfaces by assuming ideal steady flows (Ishibashi 1983). However, the assumptions of the steady flows cannot provide proper explanations for interactions between the highly concentrated sediment flows and the abrasion.

With respect to prediction methods for water-sediment mixture flows, several studies demonstrated the effectiveness of high-resolution Euler-Lagrange (HEL) strategies. In the HEL strategies, particle motions are simulated using the discrete element method (DEM) based on the Lagrangian approach, and flow motions are simulated using the Eulerian approach. In these simulations, fluid motions surrounding particles are simulated accurately by using computational grids smaller than the particles, and fluid forces are computed directly by the surrounding flow motions without the drag coefficient. The HEL

Red color particles display fracture rates γ_f of concrete spheres that determine the upper limits of tensile forces among neighboring concrete spheres.
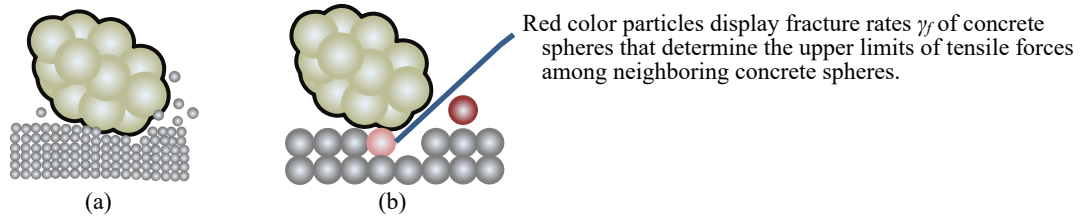
(a) (b)

Figure 1: Concept of the sub-particle abrasion model.

The left side model naturally simulates concrete fracture with small concrete spheres by using natural tensile strength of concrete. However, it requires too large computation costs for the simulation. The right side model cannot simulate directly several small particles moving out from the concrete bed, indicated in the left side figure, but can simulate these sub-particle scale abrasions by decreasing bonding forces of concrete spheres. The model implements concrete abrasion simulations with the CDEM method by using relatively large particles, and reducing computation load.

method can be a powerful tool for simulation of water and sediment motions in studies on invert concrete abrasion.

With respect to the simulations of concrete behavior, Megro and Hakuno (1989) developed a Modified DEM (MDEM) method that is capable of simulating concrete behavior by introducing a tensile force into the DEM method. From a microscopic view point, the phenomenon of concrete abrasion is one of concrete fractures. Thus, the concrete DEM (CDEM) method introducing tensile forces is presumed to be a suitable model for predicting concrete abrasion. However, if small spheres are used for simulations of concrete abraded powder, too many concrete spheres are necessary for the simulation as illustrated Fig. 1(a). This makes implementation of the simulation difficult due to the large computational load. On the other hand, if large spheres are used, collision forces are averaged in a large space depending on sphere sizes and, estimated on average as smaller forces than those in the contact scale. In this case concrete is difficult to fracture without receiving extremely large collision forces. To prevent these problems, concrete abrasion simulations in the DEM require sub-particle scale abrasion models that are capable of simulating abrasion behavior in smaller scale than particles.

Fukuoka *et al*. (2014) developed the APM (Arbitrary Particle Multiphase) code based on the HEL strategy using the finite difference method and Cartesian computation grids for the flow simulation. This method can simulate motions of arbitrarily-shaped particles, in which particles of various shapes are made by superimposing several small spheres. It was confirmed in a study (Fukuda and Fukuoka 2016) that the validation of flows and particle motions simulated by the APM was achieved by comparing them with those measured in debris flow laboratory experiments conducted by Egashira *et al*. (2001).

In this study, the DEM concrete model with sub-particle abrasion model was developed and added to the APM code. This simulation code is termed APM-CDEMA (APM-Concrete DEM-Abrasion). If the forces and abrasion speed are connected using a sub-particle scale abrasion model, an unnatural abrasion will progress in such a way that concrete abrasion will increase because of large contact forces from a large amount of static deposited particles. Our sub-particle scale abrasion model eliminates this unnatural

abrasion by being based on the balance between the loss of the mechanical energy of moving gravels and the energy of the concrete fracture. The validation of the developed model was examined by applying the model to the abrasion experiment conducted in a study by Fukuoka *et al.* (2004). In the experiment, large quantities of real scale gravels and water were supplied to an invert-shape concrete open channel, and concrete abrasion shapes were measured. From the comparisons of the simulated abrasion and that in the experiment, the applicability of the APM-CDEMA code as a prediction method of invert concrete abrasion was discussed.

2   Methodology of the APM

The APM code is based on the high-resolution Euler-Lagrange strategy (Fukuoka *et al.* 2014). Water motions were computed with a one fluid model for incompressible solid-liquid multiphase flow assuming solid parts as fluids of different densities and using computational grid smaller than the particles. Gravels were made by superimposing several small spheres without leaving any gaps. Contact forces among gravels were computed by the DEM with small spheres composing gravel by using springs, dashpots and frictional sliders. Motions of gravels were simulated as rigid bodies. For more details, refer to Fukuoka *et al.* (2014).

3   Concrete abrasion model

3.1   Relations between concrete abrasion and fracture in the abrasion model

The sub-particle scale abrasion model takes into account the energy balance between the loss of the mechanical energy of moving gravels and the energy consumed to fracture concrete in the DEM method. Ishibashi (1983) linked the abrasion volume and loss of the mechanical energy of moving particles with an abrasion coefficient, as follows:

$$\Delta V_w = C_w \Delta E_{nm} \tag{1}$$

where ΔV_w is the abrasion volume, C_w is the abrasion coefficient, and ΔE_{nm} is the loss of the mechanical energy of moving particles. The values of the coefficients were determined by laboratory experiments under relatively steady and simple flow conditions. Thus, the value of the abrasion coefficient is presumed to be reliable. Therefore, if the energy loss of the moving particles ΔE_{nm} is predicted accurately under various conditions of abrasions and flows, the progress of abrasion is presumed to be predicted properly. Thus, the relation in Eq. [1] was introduced into the sub-particle scale abrasion model of the concrete DEM method. The concept of our sub-particle scale abrasion model is illustrated in Fig. 1(b). Eq. [1] was employed for the determination of the fracture rate of the concrete. We will discuss this method in more detail in a later section.
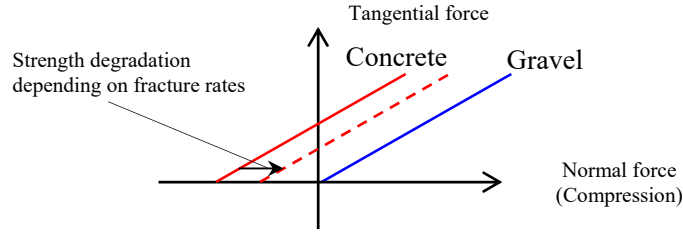
Figure 2: Yield criterion of the DEM.

The yield criterions of normal forces and tangential forces in the DEM are shown in Fig. 2. The objective of this study is not to investigate in detail the yield criterions of concrete. Thus, a simple, linear concrete yield criterion was used, indicated by the red solid line in Fig. 2. The strength degradation of concrete was computed using the fracture rate and modeled by decreasing the upper limit of the tensile force with keeping the friction angle. The upper limit for the tensile strength of the spheres composing the concrete was varied by the following equation:

$$\sigma_{t,\max} = (1 - \gamma_f)\sigma_{t,\max}^{(0)} \tag{2}$$

where $\sigma^{(0)}_{t,\max}$ and $\sigma_{t,\max}$ are the tensile strengths at the initial time and at the corresponding time, respectively. γ_f is the fracture rate. This tensile strength and the upper limit of the tensile force f_b in the DEM method depicted in Fig. 2 were linked by defining the contact area A of two concrete spheres, i and j, as follows:

$$f_b = A\frac{\sigma_{t,\max,i} + \sigma_{t,\max,j}}{2} \tag{3}$$

$$A = 4r_c^2 \tag{4}$$

where $\sigma_{t,\max,i}$ and $\sigma_{t,\max,j}$ are the tensile strengths of concrete spheres i and j, respectively; considering the strength degradations, and r_c is the radius of the concrete spheres.

3.2 Fracture rate

Concrete fracture energy, which is necessary for fracturing all parts of any concrete object, is presumed to depend on the volume of the object. Thus, we defined the energy that fractures a unit volume of concrete as C_{Ef}. Based on this relation, it is presumed that complete fracture has occurred when the sum of the energy consumed in the concrete fracture ΔE_f of volume V_Ω equals to $C_{Ef} V_\Omega$. Thus, the fracture rate γ_f was defined as follows.

$$\gamma_f = \frac{\sum \Delta E_f}{C_{E_f} V_\Omega} \tag{5}$$

The energy consumed in the concrete fracture is assumed to be the same as the energy consumed for abrasion of the same volume. This assumption allows connecting the
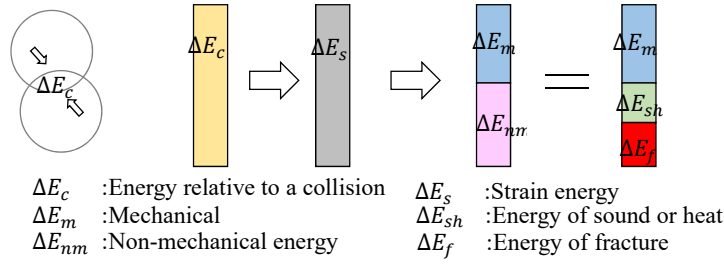
ΔE_c

ΔE_c

ΔE_c ⇨ ΔE_s ⇨ ΔE_m = ΔE_m

ΔE_{nm} ΔE_{sh}

ΔE_f

ΔE_c :Energy relative to a collision ΔE_s :Strain energy
ΔE_m :Mechanical ΔE_{sh} :Energy of sound or heat
ΔE_{nm} :Non-mechanical energy ΔE_f :Energy of fracture

Figure 3: Transfer of the energy relative to a collision.

abrasion volume ΔV_w and fracture energy ΔE_f by using the fracture energy per unit volume C_{Ef} as follows.

$$C_{E_f}\Delta V_w = \Delta E_f \qquad [6]$$

The transfer of the energy relative to a collision is depicted in Fig. 3. The non-mechanical energy ΔE_{nm}, which is the loss of the mechanical energy of the particles after collisions, is not the same as the fracture energy ΔE_f, and partially transfers into an energy ΔE_{sh} of sound and heat. In this energy transfer, we assumed that the ratio of the energy consumed in fractures to the sum of the energy consumed in fractures and the energy transferring into sound and heat was constant, and this ratio is defined $\alpha_{f,nm}$ as follows.

$$\alpha_{f,nm} = \frac{\Delta E_f}{\Delta E_f + \Delta E_{sh}} = \frac{\Delta E_f}{\Delta E_{nm}} \qquad [7]$$

The derivation of the abrasion coefficient in Eq. [1] did not consider the variation in $\alpha_{f,nm}$. Thus, the assumption of Eq. [7] is the same as the assumption for the derivation of the abrasion coefficient. By substituting Eq. [6] into Eq. [7], the following equation is obtained.

$$\Delta V_w = \frac{\alpha_{f,nm}}{C_{E_f}}\Delta E_{nm} \qquad [8]$$

By comparing Eq. [1] and Eq. [8], the following relation between the fracture energy C_{Ef} of a unit volume and the abrasion coefficient C_w is obtained.

$$C_w = \frac{\alpha_{f,nm}}{C_{E_f}} \qquad [9]$$

By substituting Eq. [7] and Eq. [9] into the definition of the fracture rate in Eq. [5], the following equation is obtained.

$$\gamma_f = \frac{\alpha_{f,nm}\sum\Delta E_{nm}}{C_{E_f}V_\Omega} = \frac{C_w\sum\Delta E_{nm}}{V_\Omega} \qquad [10]$$

Thus, when the loss of the mechanical energy of particles ΔE_{nm} is known, the fracture rate γ_f can be computed with the abrasion coefficient C_w.

The energy, transfer from the mechanical energy of contacting two particles i and j into non-mechanical energy in collisions, can be obtained by the following equation:

(a) Full view of the experimental setup | (b) Sediment supplying section. | (c) Abraded concrete invert after 3,500m³ sediment was supplied
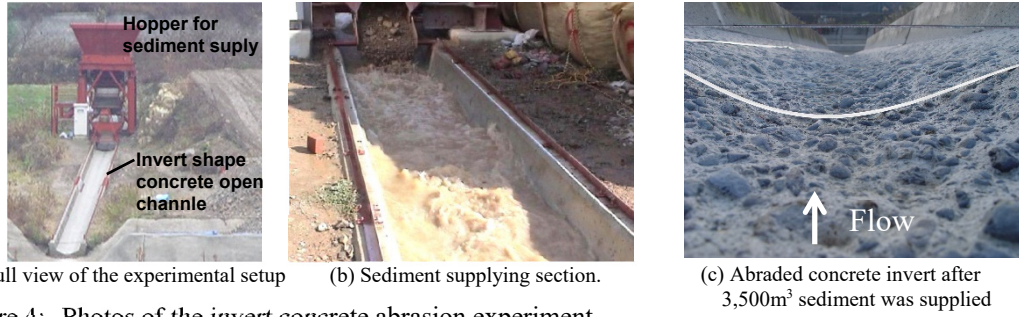
Figure 4: Photos of the invert concrete abrasion experiment.

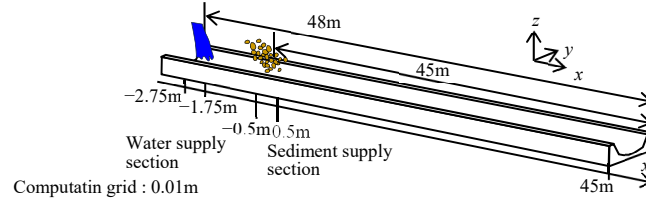
Figure 5: Numerical setup.
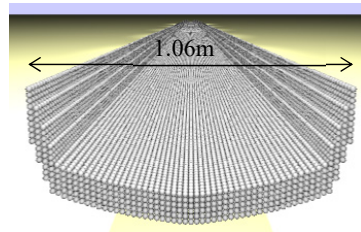
Figure 6: Arrangement of concrete spheres in a cross section.

$$\Delta E_{nm,ij} = \boldsymbol{f}_{c,i} \cdot (\boldsymbol{v}_j - \boldsymbol{v}_i)\Delta t \qquad [11]$$

where $\boldsymbol{f}_{c,i}$ is the contact force vector from the particle j to the particle i, $\boldsymbol{v}_i$ and $\boldsymbol{v}_j$ are the velocity vectors of contacting points of the particles i and j. When the material strain energy of the particles is converted into mechanical energy, $\Delta E_{nm,ij}$ becomes a negative value. However, mechanical energy is not produced during one total collision. Therefore, the sum of $\Delta E_{nm,ij}$ becomes a positive value and is able to be used for predicting the loss of the mechanical energy of particles. In the simulation, this $\Delta E_{nm,ij}$ was divided with respect to particles i and j as $\Delta E_{nm} = 0.5\Delta E_{nm,ij}$, respectively.

4 Simulation of invert concrete abrasion experiment

4.1 Numerical setup

Fukuoka *et al*. (2004) conducted an experiment on invert concrete abrasion. In the experiment, a 45 m long invert-shape concrete open channel with a bed slope of 1:20 was used. A large quantity of gravels and water were supplied from the upstream, and changing shapes of the invert bottom due to the abrasion were measured. Figure 4 shows a full view of the experimental set up (left), a view of the sediment supplying section (middle) and the abraded invert bottom (right). The developed APM-CDEMA code was used in the simulation of this invert concrete abrasion experiment. From a comparison between the
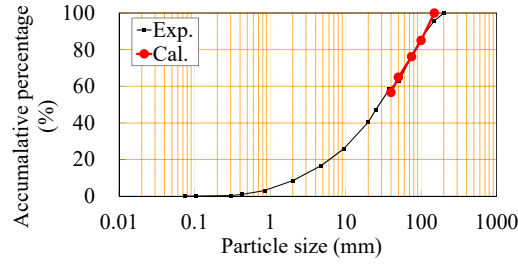
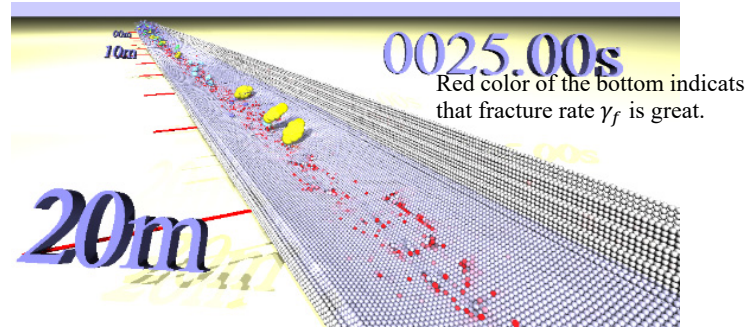Figure 7: Particle size distributions of the experiment and the simulation.

Figure 8: Snap shot of gravels, water surface and invert abrasion.

progress of concrete abrasion in the simulation and that in the experiment, the validation of the result of the APM-CDEMA was examined. The numerical set up was shown in Fig. 5. The cross sectional view of the numerical concrete invert is shown in Fig. 6. The experimental concrete invert was represented by groups of spheres of 0.02 m in the simulation. The particle size distributions of the simulation and that of the experiment were shown in Fig. 7. Particles with 5 sizes (0.04 m, 0.05 m, 0.075 m, 0.1 m, and 0.15 m) were used in the simulation. The rate of water supply was 0.5 m^3/s and that of the sediment was 0.0083 m^3/s, same as in the experiment. Although, the experiment was performed for 80 hours, we could only simulate the first 33.3 hours in the experiment because of large computational load. Moreover, we shortened 33.3 hours of the experimental time to 25 s of the simulation time. To compare the simulated abrasion with that of the experiment, the non-mechanical energy ΔE_{nm} in Eq. [11] was multiplied by the acceleration parameter β (= 4,800($\simeq$ 33.3×60×60/25)). The abrasion coefficient $C_w = 1.1\times10^{-7}$ m^3/J and the initial tensile strength $\sigma^{(0)}_{t,\max} = 2.7\times10^6$ (Pa), which was 1/12 the compressive strength of the experimental invert-concrete, were used in the simulation.

4.2 Comparison between the abrasion in the simulation and those in the experiment

A Snap shot of gravel, water surface and invert concrete abrasion in the simulation is depicted in Fig. 8. Fracture rate of the concrete is shown as red color. Large fracture rates prevailed in a wide range of the channel bottom, which implied that sub-particle scale abrasion model has great effect on the abrasion simulation. Because of the short

* The abrasion depth in the simulation was measured by determining radii of the abraded concrete spheres as $(1-\gamma_f)r_c$.
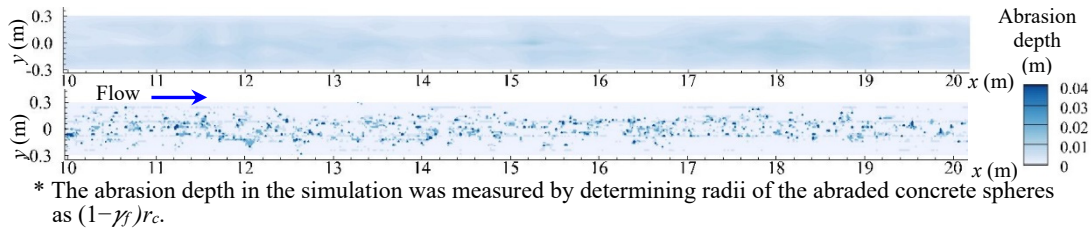
Figure 9: Contour of the abrasion depth
(Top: Experiment (At the time of the sediment volume of 245 m³ supplied), Bottom: Simulation (At the time of the converted sediment of 91 m³ having passed the section x = 10 m))
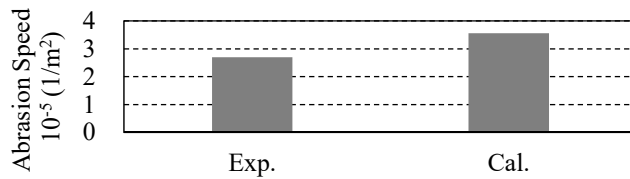

Figure 10: Abrasion speed at the center of the channel.

simulation time of 25 s, at the end of the simulation, many particles still remained at the supplying section. Therefore, we compared concrete abrasion of the simulation and that of the experiment in the relatively upstream section from x = 10 m to 20 m. The abrasion-depth contour of the experiment (at the time where the supplied sediment volume was 245 m³, which is the first measurement after the sediment supply) and the simulation (at the time of the converted sediment of 91 m³ passing the x = 10 m section) are shown in Fig. 9. The sediment volume of the simulation converted to the experimental volume of 91 m³ was determined by multiplying the simulated sediment volume passing the section x = 10 m by the acceleration parameter β. Because both channel beds of the simulation and of the experiment do not yet display wavy abrasion by this amount of sediment volume, motions of the water and the sediment were not affected greatly by the abraded channel bed. A comparison of the speed of abrasion depth per unit passing sediment volume at the center of the channel in the section from x = 10 m to x = 20 m is shown in Fig. 10. The abrasion speed in the simulation matched well with that of the experiment. Therefore, simulated moving particle, concentrating on the center of the channel, and the relation between the progress of the abrasion and the particle motions presumed to be a good match with those in the experiment.

5   Conclusion

In this paper, APM-CDMA code was developed, in which motions of water and particles were simulated in the HEL strategies, and concrete was simulated in the CDEM method with the new sub-particle scale abrasion model. The developed APM-CDEMA code was applied to the experiment of the invert concrete abrasion (Fukuoka *et al*. 2004). Because the simulation time was still short, the model validation could be examined with only the early stage of the abrasion in the experiment, in which bed waves of the invert due to the

abrasion were not confirmed yet. The examination brought that the abrasion speed simulated with the APM-CDEMA code agreed well with that of the experiment in the early stage of the invert abrasion. We will perform this simulation for longer time hereafter, and further validations should be checked. The APM-CDEMA code is capable of simulating complicated interactions between motions of sediment flows and the abrasion. This HEL strategy is expected to be a powerful tool for predicting the invert concrete abrasion.

References

Ishibashi, T. (1983). A hydraulic study on protection for erosion of sediment flush equipments of dams, *Proc. JSCE,* 334(6), 103–112 (in Japanese).

Egashira S., Itoh T., Takeuchi H. (2001). Transition mechanism of debris flows over rigid bed to over erodible bed, *Phys.Chem. Earth (B)*, 26(2), 169-174.

Megro, K., Hakuno, M. (1989). Fracture analyses of concrete structures by the modified distinct element method. *Proc. JSCE*, 410, 113-124.

Fukuoka, S., Shinohara, Y., Masaki, J. (2004). Shigemura, K., Todo, M., Okada, S., Saito, K. : Experimental study on the development mechanism of abrasion in a concrete channel invert due to flushing sediment-laden flow., *Proc. Hydraul. Eng*., 48, 1135-1140 (In Japanese).

Fukuoka, S., Fukuda, T., Uchida, T. (2014). Effects of sizes and shapes of gravel particles on sediment transports and bed variations in a numerical movable-bed channel, *Adv. Water Resour.*, 72, 84-96.

Fukuda, T., Fukuoka S. (2016). Euler-Lagrange simulations of debris flow experiments, *Proc. Two-pHase modElling for Sediment dynamIcS in geophysical flows THESIS-2016*, Tokyo – Japan, 17-20.

Authors

Tomoo Fukuda (corresponding Author)
Shoji Fukuoka
Research and Development Initiative, Chuo University, 1-13-27 Kasuga, Bunkyo-ku, Tokyo 112-8551, Japan
Email: t-fukuda@tamacc.chuo-u.ac.jp